Biochemical and Biophysical Research Communications 451 (2014) 126–130

Contents lists available at ScienceDirect

Biochemical and Biophysical Research Communications

journal homepage: www.elsevier.com/locate/ybbrc

Crystal structures of type III_H NAD-dependent D-3-phosphoglycerate dehydrogenase from two thermophiles

S.M. Kumar [a], K.J. Pampa [b], M. Manjula [a], G. Hemantha Kumar [c], Naoki Kunishima [d], N.K. Lokanath [a,*]

[a] Department of Studies in Physics, University of Mysore, Mysore 570 006, India
[b] Department of Studies in Microbiology, University of Mysore, Mysore 570 006, India
[c] Department of Studies in Computer Science, University of Mysore, Mysore 570 006, India
[d] Advanced Protein Crystallography Research Group, RIKEN SPring-8 Center, Harima Institute, Hyogo 679-5148, Japan

ARTICLE INFO

Article history:
Received 7 July 2014
Available online 24 July 2014

Keywords:
PGDH
NAD^+
Substrate binding domain
Nucleotide binding domain

ABSTRACT

In the L-Serine biosynthesis, D-3-phosphoglycerate dehydrogenase (PGDH) catalyzes the inter-conversion of D-3-phosphoglycerate to phosphohydroxypyruvate. PGDH belongs to 2-hydroxyacid dehydrogenases family. We have determined the crystal structures of PGDH from *Sulfolobus tokodaii* (*St*PGDH) and *Pyrococcus horikoshii* (*Ph*PGDH) using X-ray diffraction to resolution of 1.77 Å and 1.95 Å, respectively. The PGDH protomer from both species exhibits identical structures, consisting of substrate binding domain and nucleotide binding domain. The residues and water molecules interacting with the NAD are identified. The catalytic triad residues Glu-His-Arg are highly conserved. The residues involved in the dimer interface and the structural features responsible for thermostability are evaluated. Overall, structures of PGDHs with two domains and histidine at the active site are categorized as type III_H and such PGDHs structures having this type are reported for the first time.

1. Introduction

D-3-phosphoglycerate dehydrogenase (PGDH, EC 1.1.1.95) is involved in the biosynthesis of L-Serine using NAD^+ cofactor for the inter-conversion of D-3-phospoglycerate to phospohydroxy-pyruvate. Serine is essential for the synthesis of biomolecules (and proteins) needed for cell proliferation including nucleotides, sphingosine and phosphatidyl-serine [1]. This enzyme belongs to the 2-hydroxyacid dehydrogenases family, and shares sequence similarity with glyoxylate reductases, formate dehdydrogenases, D-lactate and D-glycerate dehdydrogenases. The NAD-dependent hydroxyacid dehydrogenases play major roles in the carbohydrate metabolism, oxidation of NADH to NAD^+, and act as catalyzing agent in the reversible conversion of keto acids into chiral hydroxy acids [2,3]. Generally, the structures of PGDH are mainly classified as type I, type II, type III_H and type III_K, depending on the number of domains and the residues at the active site. *Escherichia coli* [4,5] and *Mycobacterium tuberculosis* [6,7] PGDH belong to type I and type II structures, respectively. And, these enzymes consist of three domains; substrate binding domain (SBD), nucleotide binding domain (NBD) and an additional regulatory domain (exists as tetramer). Whereas, type III PGDH consists of two domains (NBD and SBD), which are resolved into type III_H (histidine) and type III_K (lysine) depending on the presence of active site residue (exist as dimer) [8].

In the present study we present crystal structures of NAD dependent PGDH from *Sulfolobus tokodaii* (*St*PGDH) and *Pyrococcus horikoshii* (*Ph*PGDH) using X-ray diffraction to resolution of 1.77 Å and 1.95 Å, respectively. The polypeptide chain of *St*PGDH and *Ph*PGDH is assembled into two domains (NBD and SBD) with histidine at the active site, belonging to type III_H [8]. Dimeric structure is observed with subunit–subunit interactions of the NBD domains. The structure based multiple sequence alignment of PGDH sequences result in the presence of a nucleotide binding motif, which has a consensus sequence *G-X-G-X-X-G* [9] (Supplemental Fig. S1).

2. Materials and methods

2.1. Protein expression and purification

The plasmid encoding *St*PGDH protein is digested with *Nde*I and the fragment were inserted into the expression vector pET-21a linearized with *Nde*I and *Bam*HI. The recombinant plasmid were transformed into *Escherichia coli* BL21 (DE3) cells and was grown at 310 K in Luria–Bertani medium containing 0.5 μg ml^{-1} ampicillin for 20 h. The cells were harvested by centrifugation at

* Corresponding author. Fax: +91 821 2419333.
E-mail address: lokanath@physics.uni-mysore.ac.in (N.K. Lokanath).

http://dx.doi.org/10.1016/j.bbrc.2014.07.075
0006-291X/

6500 rev min^{-1} for 5 min at 277 K. The cell pellet was suspended in 20 mM Tris–HCl pH 8.0 containing 0.5 M sodium chloride and 5 mM 2-mercaptoethanol and was then homogenized by ultrasonication. The supernatant was heated at 343 K for 12 min and the cell debris and denaturated protein were then removed by centrifugation (14,000 rev min^{-1}, 30 min); the supernatant solution was used as the crude extract for purification. The crude extract was desalted with a HiPrep 26/10 desalting column and applied onto a Super Q Toyopearl 650 M column equilibrated with 20 mM Tris–HCl pH 8.0. The fraction containing proteins were eluted with a linear gradient of 0–0.3 M sodium chloride. Proteins were then dialyzed against 20 mM Tris–HCl pH 8.0 and subjected to a Resource Q column (Amersham Biosciences) equilibrated with 20 mM Tris–HCl pH 8.0. Fractions containing proteins were again eluted with a linear gradient of 0–0.3 M sodium chloride. The protein was desalted with a HiPrep 26/10 desalting column with 10 mM sodium phosphate pH 7.0 and applied onto a Bio-Scale CHT20-I column (Bio-Rad) equilibrated with 10 mM sodium phosphate pH 7.0. Proteins were again eluted with a linear gradient of 10–150 mM sodium phosphate. Later same was desalted with a HiPrep 26/10 desalting column with 20 mM Tris–HCl pH 8.0 containing 0.05 M sodium chloride and applied onto a Mono Q column (Amersham Biosciences) equilibrated with 20 mM Tris–HCl pH 8.0 containing 0.05 M sodium chloride. The fraction containing protein was eluted with a linear gradient of 0–0.5 M sodium chloride. The fraction containing proteins were cooled, concentrated by ultrafiltration (Vivaspin, 10 kDa cutoff) and loaded onto a HiLoad 16/60 Superdex 75 pg column (Amersham Biosciences) equilibrated with 20 mM Tris–HCl pH 8.0 containing 0.05 M sodium chloride. The homogeneity and identity of the purified sample were estimated by SDS–PAGE and N-terminal sequence analysis. Protein concentrations were determined using UV method and Bio-Rad protein assay based on the Bradford dye-binding procedure, using bovine serum albumin as standard. Finally, the purified *St*PGDH was concentrated to 18.0 mg ml^{-1} by ultrafiltration and stored at 203 K. Similarly, we purified *Ph*PGDH protein (*Bgl*II and pET-11a) with a concentration of 17.0 mg ml^{-1}.

The oligomeric state of purified *St*PGDH and *Ph*PGDH were examined by a dynamic light-scattering experiment performed using DynaPro MS/X instrument (Protein Solutions). The measurements were measured at 291 K on the purified protein at 1 mg/ml in buffer solution containing 20 mM Tris–HCl and 200 mM sodium chloride.

2.2. Crystallization

The crystals of *St*PGDH were grown at room temperature by sitting-drop method by mixing equal volumes (1 μl) of protein solution and reservoir solution. The solution consisted of 0.1 M ammonium sulfate, pH 6.0 and 20% (w/v) polyethylene glycol 4000. And the crystals of *Ph*PGDH were grown at room temperature by sitting-drop method by mixing equal volumes (1 μl) of protein solution and reservoir solution. The solution consisted of 0.1 M sodium cacodylate, pH 5.8 and 40% (w/v) polyethylene glycol 4000.

2.3. Data collection and processing

X-ray intensity data sets were collected at the synchrotron beam line BL26B1 at SPring-8, Japan, under cryogenic conditions. Crystals were flash-frozen with liquid nitrogen at 100 K in their respective mother liquor or soaking solution containing 30% (v/v) glycerol as cryoprotectant. The RIGAKU IP detector was used for data collection. Each frame was exposed for 45 s with a 1° oscillation at a crystal-to-detector distance of 250 mm. The data were indexed and scaled with the HKL package [10]. The datasets were completed by including all possible *hkl* and R_{free} columns using UNIQUE of CCP4 suite [11]. Care was taken to keep the same R_{free} flags in all datasets. Structure factors were calculated using CCP4 suite. Data collection parameters and processing statistics are summarized in Table 1.

2.4. Structure determination

The structure of *St*PGDH was solved using molecular replacement method [12]. The trimmed model of *Human* PGDH (PDB code: 2G76; unpublished data) was used as the search model to perform molecular replacement. The sequence identity between *St*PGDH and *Hu*PGDH was 36%. To minimize the bias caused by the search model, we modified the search model based on the sequence alignment. Low sequence similarity and sequence gaps were eliminated from the model. The orientation of the search model was determined by a fast rotation function calculated using CNS [13] and gave a clear solution in the space group *C*2.

The structure of *Ph*PGDH was solved by multiwavelength anomalous dispersion method [14]. Se-atom positions were obtained with the program SOLVE [15] and the initial electron density map was calculated by SOLVE/RESOLVE [15]. Solvent flattening

Table 1
Summary of crystal data, data collection and refinement statistics of *St*PGDH and *Ph*PGDH.

Data statistics	*St*PGDH	*Ph*PGDH
Space group	*C*2	$P2_1$
Unit-cell parameters (Å,0)	a = 105.07, b = 59.8, c = 60.73; β = 114.3	a = 91.76, b = 63.74, c = 131.98; β = 103.14
V_M ($Å^3$ Da^{-1})	2.5	2.5
Content of the asymmetric unit	Dimer	Dimer
Resolution (Å)	50.0–1.77 (1.83–1.77)	50.0–1.95 (2.02–1.95)
Reflections (measured/unique)	33,207/33,238	105,186/101,628
R_{merge} (%)	3.6	8.9
Completeness (%)	99.8 (98)	97 (98.9)
$\langle I/\sigma\ (I)\rangle$	19.2	6.8
Redundancy	3.0	3.8
Refinement statistics	*St*PGDH	*Ph*PGDH
Resolution (Å)	40–1.77	34.69–1.95
R_{cryst} (%)	18.8	23.5
R_{free} (%)	22.0	26.5
RMS bond lengths (Å)	0.006	0.006
RMS bond angles (°)	1.1	1.3
Ramachandran plot (%)		
Most favored	95.16	94.34
Additional	4.19	5.21
Generous	0.65	0.45

Values in parentheses are for the highest resolution shell.

and histogram matching were performed to improve the phases. Most of the secondary structural elements were interpretable in the improved map.

2.5. Crystallographic refinement and model building

All crystallographic refinements were carried out using CNS [13]. The topology and parameter files of the NAD^+ molecule was obtained from the Hetero-compound Information Center of Uppsala on the Uppsala website [16]. Stereochemical quality of both the coordinates was checked with the program PROCHECK [17]. The refinement statistics are summarized in Table 1 (*St*PGDH and *Ph*PGDH).

The final atomic coordinates of *St*PGDH and *Ph*PGDH are deposited in the RCSB Protein Data Bank (http://www.rcsb.org/pdb) with the accession codes 2EKL and 2D0I, respectively.

2.6. Model analysis

DALI [18] (http://ekhinda.biocenter.helsinki.fi/daliserver/start) server was utilized for structural similarity search against all known structures deposited in the PDB. Figures preparation of protein models was prepared using PyMol (http://www.pymol.org). Surface areas for dimer and hydrogen bonds were calculated using PISA [19]. The ionic bridges were calculated using ESBRI [20]. Aromatic–aromatic interactions and cation–pi interactions were calculated using PIC [21]. Multiple sequence alignment is performed using CLUSTALW [22] and the figure was generated using ESPript [23]. The structures were superposed using LSQKAB program, integrated in CCP4i [24].

3. Results and discussions

3.1. Overall structure

The monomer of *St*PGDH and *Ph*PGDH consists of two domains; the substrate binding domain (SBD) and nucleotide binding domain (NBD) (Fig. 1). Both monomers showed identical secondary structural elements (Table 2). However, the only difference is that, the extra insert α14 at C-terminal (SBD) and α7 (NBD) observed in *Ph*PGDH when compared to *St*PGDH (Supplemental Fig. S2). Both subunits are superimposed with a root mean square deviation (r.m.s.d) of 2.8 Å for all the 280 pairs of Cα atoms.

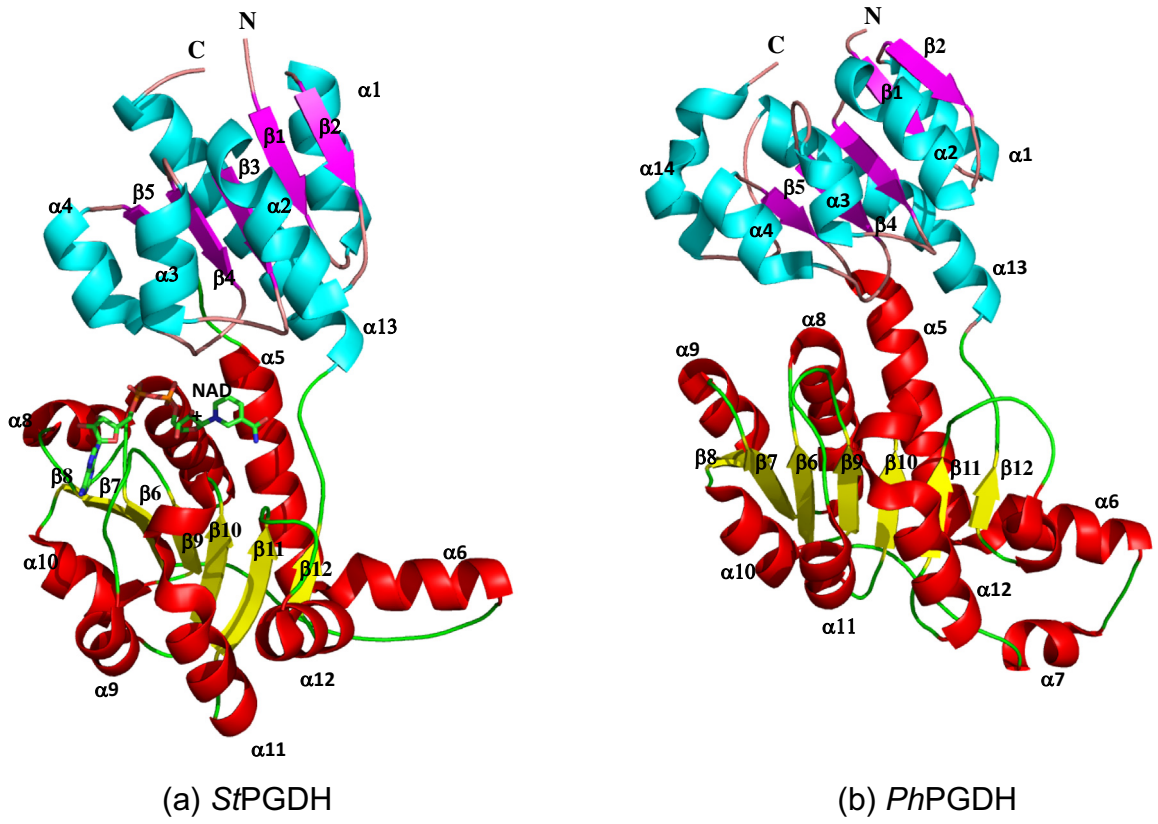

Fig. 1. Overall monomeric structure of PGDH. (a) *St*PGDH is mainly composed of SBD (residues 1–96 and 289–313) and NBD (residues 97–288). The NAD^+ is shown as stick model (green). (b) *Ph*PGDH is composed of SBD (residues 1–91 and 290–333) and NBD (residues 92–289). SBD – substrate binding domain (cyan-helices, magenta-beta sheets) and NBD – nucleotide binding domain (red-helices, yellow-beta sheets). N-terminal and C-terminal are marked correspondingly. (For interpretation of the references to colour in this figure legend, the reader is referred to the web version of this article.)

Table 2
Secondary structural elements of the monomer.

	SBD residue range secondary structures	NBD residue range secondary structures	Extra insert when compared to *St*PGDH
*St*PGDH	1–96 and 289–313 α1–α4, α13 and β1–β5	97–297 α6–α12 and β6–β12	–
*Ph*PGDH	1–90 and 290–333 α1–α4 α13–α14 and β1–β5	91–289 α6–α12 and β6–β12	α7 and α14

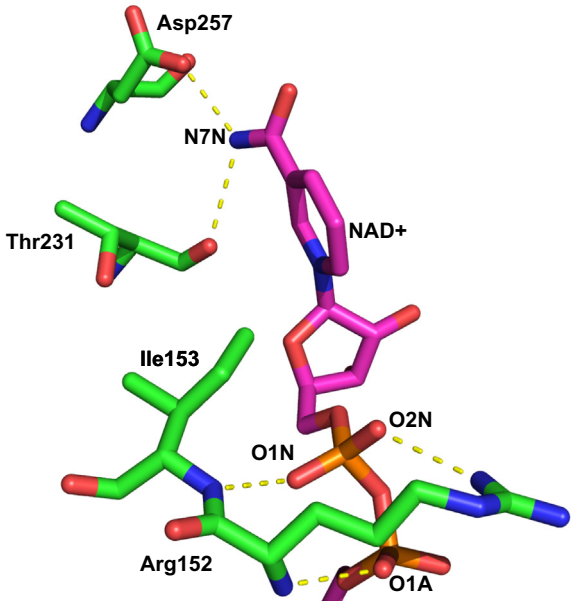

Fig. 2. Cofactor interaction with the enzyme. NAD^+ is represented by magenta stick model. The residues interacting directly with the cofactor are represented by green stick model. Yellow dotted lines indicate hydrogen bonding. (For interpretation of the references to colour in this figure legend, the reader is referred to the web version of this article.)

3.2. Oligomeric structure and thermostability

The dimeric interface between NBD domains of each protomer consists of thirtyeight (*St*PGDH) and forty hydrogen bonds (*Ph*PGDH). In addition, aromatic–aromatic (A–A), aromatic–sulfur (A–S), cation–pi (C–P) and ion pairs (I–P) are involved in the dimerization. The dimeric interfaces of *St*PGDH and *Ph*PGDH consist of three A–A, two A–S, six I–P and four A–A, four C–P, and seven I–P, respectively (Supplemental Table 1(a and b)). And their interface (dimeric) areas of *St*PGDH and *Ph*PGDH are calculated to be 2506.1 $Å^2$ and 2884.3 $Å^2$, respectively. The above interactions leading to the oligomerization can provide PGDH to perform the catalysis at higher temperature [25].

The monomeric structural features of A–A, A–S, C–P and I–P interactions contribute to the protein stability at high temperature [26] (Supplemental Table 2(a–e)). In addition, *B*-factor show low value for strand atoms when compared to helix atoms and loop atoms (Supplemental Table 3a), suggesting that the beta strands are more rigid.

Table 3
Hydrogen bonding distance between NAD^+ and the residues.

NAD^+ atom	Interacting residue	Distance in Å
O1A	Arg152 (N)	3.0
O1N	Ile153 (N)	3.0
O2N	Arg152 (NH1)	3.1
N7N	Thr231 (O)	3.1
	Asp257 (OD2)	2.7

3.3. Cofactor binding site

The electron density is clearly defined for the entire NAD^+ molecules in *St*PGDH (Supplemental Fig. S3a). The cofactor interacting with the residues of the enzyme is plotted (Fig. 2) and the distances are tab2ulated in Table 3. The N7N (of nicotinamide) hydrogen bonds to oxygen atoms of residues Thr231 and Asp257. The phosphate group atoms O1N hydrogen bonds to Ile153. The O2N and O1A atoms of cofactor hydrogen bonds to the residue Arg152. Water molecules play a major role in the interaction between

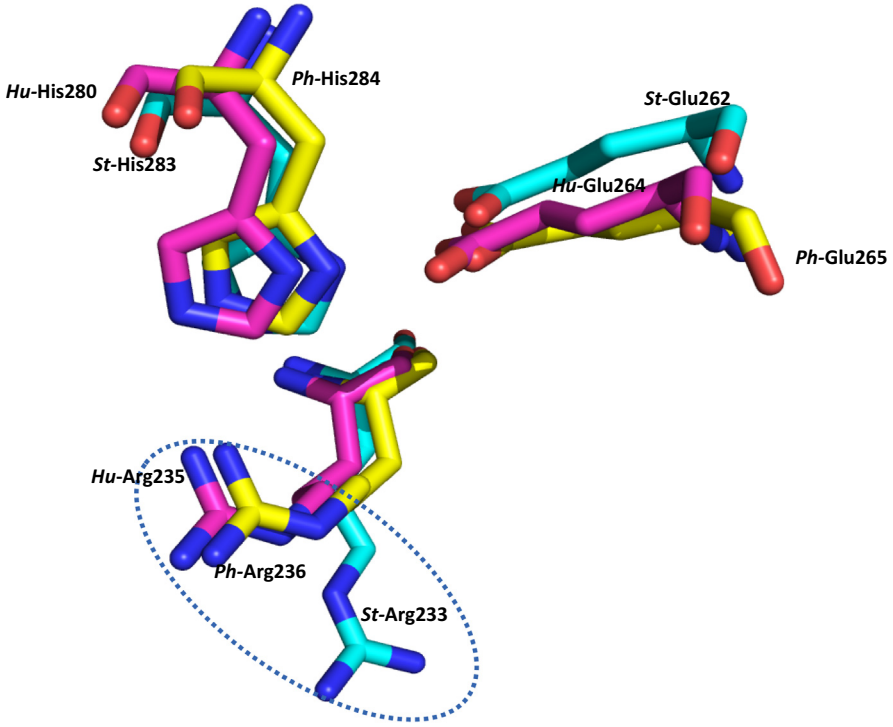

Fig. 3. Superposition of conserved catalytic residues of *Ph*PGDH (yellow stick model), *St*PGDH (cyan stick model) and *Human* PGDH (magenta stick model). Dotted line (blue) indicates the change in conformation of Arg233 (*St*PGDH). (For interpretation of the references to colour in this figure legend, the reader is referred to the web version of this article.)

cofactor and residues (Supplemental Fig. S3b; Table 3b). The water molecules (Hoh1649 and Hoh1520) form a cyclic proton relay forming hydrogen bonds to N6A and N7A atoms of adenine moiety and to the residue Thr205. Also, Thr205 is interacting with O2A through the water molecule Hoh1387. The O7N atom of the nicotinamide moiety is primarily hydrogen bonded to Hoh1327, from there to Ala286 and His283. The O4D atom is interacting with residues His203 and Thr231 through the water molecule Hoh1316. A trifurcated hydrogen bonding is observed among water molecule (Hoh1306) and residues (His203, Gly154 and Gly151). Also, this water molecule hydrogen bonds with the atom cofactor O1N. The water molecule Hoh1319 bridges between Thr102 and O2N. Similarly, the Hoh1519 bridges between atom O3D and Arg233. Overall, the residues Gly151, Arg152, Ile153 and Gly154 found in the consensus NAD binding motif (G_{149}-X_{150}-G_{151}-Arg_{152}-Ile_{153}-G_{154}) are forming hydrogen bonds (direct or through water molecules) with cofactor indicating the importance of consensus sequence.

3.4. Catalytic residues His-Glu-Arg

The catalytic dyad residues His (283/284) – Glu (262/265) with the substrate conformer Arg (233/236) (*St*PGDH/*Ph*PGDH) are highly conserved (Supplemental Fig. S1a). These invariant residues are superposed with the residues of *Human* PGDH (*Hu*PGDH), (unpublished PDB code 2G76) [7], (Fig. 3), a ternary complex. The conformation of catalytic triad residues apo-PGDH (*Ph*PGDH), holo-complex (*St*PGDH) and ternary complex (*Hu*PGDH) are compared, the catalytic dyad (His-Glu) shows the same conformation, whereas, the side chain of Arg233 (*St*PGDH) faces away when compared to Arg235 (*Hu*PGDH) and Arg236 (*Ph*PGDH). The catalytic dyad (His-Glu) shows ionic interaction in both the PGDHs (Supplemental Table 2(a and b)).

3.5. Structural comparisons

A 3-D structural similarity search using DALI server was performed for *St*PGDH and *Ph*PGDH coordinates with the available structures of the Protein Data Bank (PDB), which revealed several enzymes categorized under PGDH family fold with *Z* scores of 35.4–30.7 and with r.m.s.d. values of 2.4–3.1 Å. The enzyme *St*PGDH shows highest similarity to PGDH (unpublished PDB code 1WWK, Supplemental Table 4). Whereas, *Ph*PGDH is similar to NADP dependent Glyoxylate reductases dehydrogenase of *Pyrococcus horikoshii* (PDB: 2DBQ, *Z*-score 39.9; r.m.s.d. 3.0, 40% sequence identity), which is also a member of 2-hydroxyacid dehydrogenase family [27]. The homologous structures of PGDH are tabulated with sequence identity, r.m.s.d. and aligned residues for *St*PGDH and *Ph*PGDH (Supplemental Table 4(a and b)).

Acknowledgments

Authors would like to thank the beamline staff for assistance during data collection at beamline BL26B1 of SPring-8, Japan. The authors would like thank the IOE single crystal X-ray diffraction facility, University of Mysore, Mysore. One of the authors, S. Madan Kumar thanks UGC-BRS for providing RFSMS fellowship.

Appendix A. Supplementary data

Supplementary data associated with this article can be found, in the online version, at http://dx.doi.org/10.1016/j.bbrc.2014.07.075.

References

[1] K. Snell, Enzymes of serine metabolism in normal, developing and neoplastic rat tissues, Adv. Enzyme Regul. 22 (1984) 325–400.
[2] W. Hummel, Large-scale applications of NAD(P)-dependent oxidoreductases: recent developments, TIBTECH 17 (1999) 487–492.
[3] S. Kochhar, P.E. Hunziker, P. Leong-Morgenthaler, H. Hottinger, Evolutionary relationship of NAD+-dependent D-lactate dehydrogenase: comparison of primary structure of 2-hydroxy acid dehydrogenases, Biochem. Biophys. Res. Commun. 184 (1992) 60–66.
[4] G.A. Grant, D.J. Schuller, L.J. Banaszak, A model for the regulation of D-3-phosphoglycerate dehydrogenase, a Vmax-type allosteric enzyme, Biochem. Biophys. Res. Commun. 165 (1996) 1371–1374.
[5] D. Schuller, G.A. Grant, L. Banaszack, The allosteric site in the Vmax-type cooperative enzyme phosphoglycerate dehydrogenase, Nat. Struct. Biol. 2 (1995) 69–76.
[6] S. Dey, G.A. Grant, J.C. Scchettini, Crystal structure of *Mycobacterium tuberculosis* D-3-phosphoglycerate dehydrogenase: extreme asymmetry in a tetramer of identical subunits, J. Biol. Chem. 280 (2005) 14892–14899.
[7] S. Dey, R.L. Burton, G.A. Grant, J.C. Saccettini, Structural analysis of substrate and effector binding in *Mycobacterium tuberculosis* D-3-phosphoglycerate dehydrogenase, Biochemistry 47 (2008) 8271–8282.
[8] G.A. Grant, Contrasting catalytic and allosteric mechanisms for phosphoglycerate dehydrogenase, Arch. Biochem. Biophys. 519 (2012) 175–185.
[9] R.K. Wierenga, M.C.H. De Maeyer, W.G.J. Hol, Interaction of pyrophosphatase moieties with alpha-helixes in dinuceotide binding proteins, Biochemistry 24 (1985) 1346–1357.
[10] Z. Otwinowski, W. Minor, Processing of X-ray diffraction data collected in oscillation mode, Methods Enzymol. 276 (1997) 307–326.
[11] Collaborative Computational Project, The CCP4 suite: programs for protein crystallography, Acta Cryst. Number 4 (1994) D50 760–763.
[12] A.J. McCoy, R.W. Grosse-Kunstleve, L.C. Storoni, R.J. Read, Likelihood-enhanced fast translation functions, Acta Cryst. D61 (2005) 458–464.
[13] A.T. Brunger, P.D. Adams, G.M. Clore, W.L. DeLano, P. Gross, R.W. Grosse-Kunstleve, J.S. Jiang, J. Kuszewski, M. Nilges, N.S. Pannu, L.M. Rice, T. Simson, G.L. Warren, Crystallography and NMR system: a new software suite for macromolecular structure determination, Acta Cryst. D54 (1998) 905–921.
[14] W.A. Hendrickson, J.R. Horton, D.M. LeMaster, Selenomethionyl proteins produced for analysis by multiwavelength anomalous diffraction (MAD): a vehicle for direct determination of three-dimensional structure, EMBO 9 (1990) 1665–1672.
[15] T.C. Terwilliger, J. Berendzen, Automated MAD and MIR structure solution, Acta Cryst. D55 (1999) 849–861.
[16] G.J. Kleywegt, T.A. Jones, Databases in protein crystallography, Acta Cryst. D54 (1998) 1119–1131.
[17] R.A. Laskowski, M.W. MacArthur, D.S. Moss, J.M. Thornton, PROCHECK: a program to check the stereochemical quality of protein structures, J. Appl. Cryst. 26 (1993) 283–291.
[18] L. Holm, C. Sander, Dali: a network tool for protein structure comparison, Trends Biochem. Sci. 20 (1995) 478–480.
[19] E. Krissinel, K. Henrick, Detection of protein assemblies in crystals, in: Berthold Mrea (Ed.), Computational Life Sciences, Springer, Heidelberg, Berlin, 2005, pp. 163–174.
[20] (a) S. Kumar, R. Nussinov, Salt bridge stability in monomeric proteins, J. Mol. Biol. 293 (1999) 1241–1255;
(b) S. Kumar, C.J. Tsai, B. Ma, R. Nussinov, Contribution of salt bridges toward protein thermostability, J. Biomol. Struct. Dyn. 1 (2000) 79–85;
(c) S. Kumar, R. Nussinov, Relationship between ion pair geometries and electrostatic strengths in proteins, Biophys. J. 83 (2002) 15595–15612;
(d) J.N. Sarakatsannis, Y. Duan, Statistical characterization of salt bridges in proteins, Proteins 60 (2005) 732–739.
[21] K.G. Tina, R. Bhadra, R. Srinivasan, PIC: protein interactions calculator, Nucl. Acids Res. 35 (2007) W473–W476.
[22] J.D. Thompson, D.G. Higgins, T.J. Gibson, CLUSTAL W: improving the sensitivity of progressive multiple sequence alignment through sequence weighting, position-specific gap penalties and weight matrix choice, Nucl. Acids Res. 22 (1994) 4673–4680.
[23] P. Gouet, E. Courcelle, D.I. Stuart, ESPript: analysis of multiple sequence alignments in PostScript, Bioinformatics 15 (1999) 305–308.
[24] The CCP4 suite: programs for protein crystallography Collaborative Computational Project, Number 4, Acta Cryst. D50 (1994) 760–763.
[25] N.K. Lokanath, I. Shiromizu, N. Ohshima, Y. Nodakke, M. Sugahara, S. Kuramitsu, M. Miyano, N. Kunishima, Structure of aldolase from *Thermus thermophilus* HB8 showing the contribution of oligomeric state to thermostability, Acta Cryst. D60 (2004) 1816–1823.
[26] B. Bagautdin, K. Yutani, Structure of indole-3-glycerol phosphate synthase from *Thermus thermophilus* HB8: implications for thermal stability, Acta Cryst. D67 (2007) 1054–1064.
[27] S. Yoshikawa, R. Arai, Y. Kinoshita, T. Uchikubo-Kamo, T. Wakamatsu, R. Akasaka, R. Masui, T. Teada, S. Kuramitsu, M. Shirouzu, S. Yokoyama, Structure of archaeal glyoxylate reductase from *Pyrococcus horikoshii* OT3 complexed with nicotinamide adenine dinucleotide phosphate, Acta Cryst. D63 (2007) 357–365.